

# Direct Characterization of Plasmonic Slot Waveguides and Nanocouplers

*Andrei Andryieuski<sup>†\*</sup>, Vladimir A. Zenin<sup>‡\*</sup>, Radu Malureanu<sup>†</sup>, Valentyn S. Volkov<sup>‡</sup>, Sergey I. Bozhevolnyi<sup>‡</sup>, and Andrei V. Lavrinenko<sup>†</sup>*

<sup>†</sup>DTU Fotonik, Technical University of Denmark, Ørstedss pl. 343, Kongens Lyngby DK-2800, Denmark

<sup>‡</sup>Department of Technology and Innovation, University of Southern Denmark, Niels Bohrs Alle 1, Odense M DK-5230, Denmark

\* E-mail: [andra@fotonik.dtu.dk](mailto:andra@fotonik.dtu.dk)

\* E-mail: [zenin@iti.sdu.dk](mailto:zenin@iti.sdu.dk)

## Supporting information

**Numerical simulation and optimization.** Simulations are done in CST Microwave Studio<sup>1</sup> with the time-domain finite-integrals method. A hexahedral mesh with the mesh refinement around the slot waveguide is used. The simulation domain consists of a thick silica substrate (3  $\mu\text{m}$ ), waveguide, antenna and thick air superstrate (4  $\mu\text{m}$ ) (Figure S1a). Gold is described with the Drude formula<sup>2</sup> with plasma frequency  $1.36 \times 10^{16} \text{ s}^{-1}$  and collision frequency  $1.57 \times 10^{14} \text{ s}^{-1}$ . The dielectric substrate has a refractive index  $n = 1.47$ . A plane wave is used for the excitation

of the structure. The boundary conditions are perfect electric conductor (PEC) in the x-, and open (perfectly matched layers) in y- and z-directions. To ensure the absence of coupling to the mirror images of antennas at the PEC x- boundaries, the lateral size of the simulation domain is  $11\ \mu\text{m}$ , the longitudinal size is  $9\ \mu\text{m}$  (for calculations of the effective area and optimization) or  $19\ \mu\text{m}$  (for calculations of the electromagnetic fields). Typical simulation with a 12 CPUs (3.5 GHz), 48 GB RAM personal computer takes 1 hour. Numerical optimization with maximization of the effective area as a goal was done with the Nelder-Mead simplex algorithm with the parameters variation range  $\pm 25\%$  from the initial values. The initial values were selected through maximization of the effective area for all parameters one-by-one variation. The optimal parameters are shown in Table S1 with the geometrical parameters marked in Figure S1b,c.

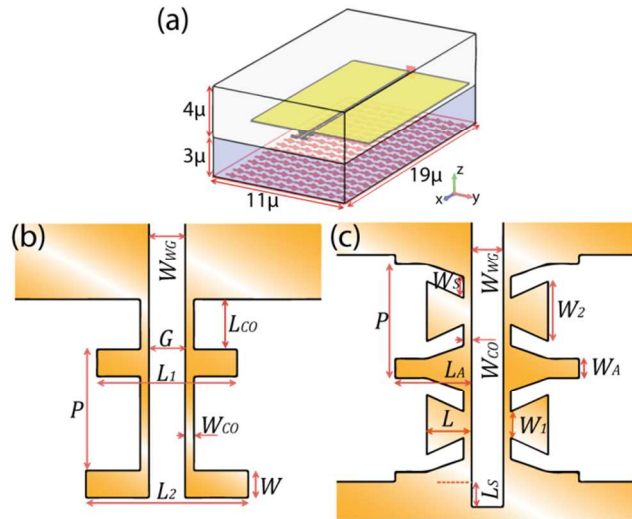


**Figure S1.** (a) Simulation domain used for the fields calculation in CST Microwave Studio. In case of effective area calculation the longitudinal size of the domain was  $9\ \mu\text{m}$  instead of  $19\ \mu\text{m}$ . Optimized serially connected (b) dipole and (c) modified bow-tie antennas. The values of optimal geometrical parameters are presented in the Table S1.

Initially we observed spurious Fabry-Perot resonances in the effective area spectra due to poorly absorbed scattered field by a single-mode plane wave port in CST (the excitation plane wave is shown with arrows in Figure S1a). This issue has been resolved by increasing the number of the port modes to 20 and proper time windowing of the received signal. The electric field recorded with a frequency 3D monitor was collected 50 nm above the top waveguide surface, corresponding to the average position of the s-SNOM tip in experiments. In order to reduce the influence of the fake Fabry-Perot resonances on the simulated electric field, the width of the excitation port was decreased to 4  $\mu\text{m}$ .

**Table S1.** Waveguide and nanocouplers geometrical parameters, designed and fabricated.

Parameter	Designed	Fabricated	St. deviation
All structures			
$H$ (nm)	50	50	1
Waveguide			
$W_{WG}$ (nm)	300	287	7
Dipole antennas coupler (2DA)			
$L_1$ (nm)	1144	1117	8
$L_2$ (nm)	1290	1293	10
$G$ (nm)	290	288	5
$W$ (nm)	210	213	6
$L_{CO}$ (nm)	443	396	10
$W_{CO}$ (nm)	80	82	8
$P$ (nm)	969	969	8
Bow-tie antenna coupler (2BA)			
$L$ (nm)	437	425	10
$W_1$ (nm)	233	246	12
$W_2$ (nm)	560	562	13
$L_A$ (nm)	683	647	7

$W_A$ (nm)	70	74	11
$W_{CO}$ (nm)	76	74	8
$W_S$ (nm)	230	200	17
$L_S$ (nm)	230	234	4
$P$ (nm)	1069	1071	20

Upon the incident wave's diffraction through the slot the surface plasmon polaritons (SPPs) are excited on the metal-dielectric interfaces. We use SPPs on metal-air interface to normalize the intensity of the slot mode. Numerical simulations (see Figure S2) confirm that the amplitude of the excited metal-air SPP does not significantly depend on the wavelength in the range of interest 1425-1525 nm and therefore the normalized slot mode intensity is proportional to the effective area.

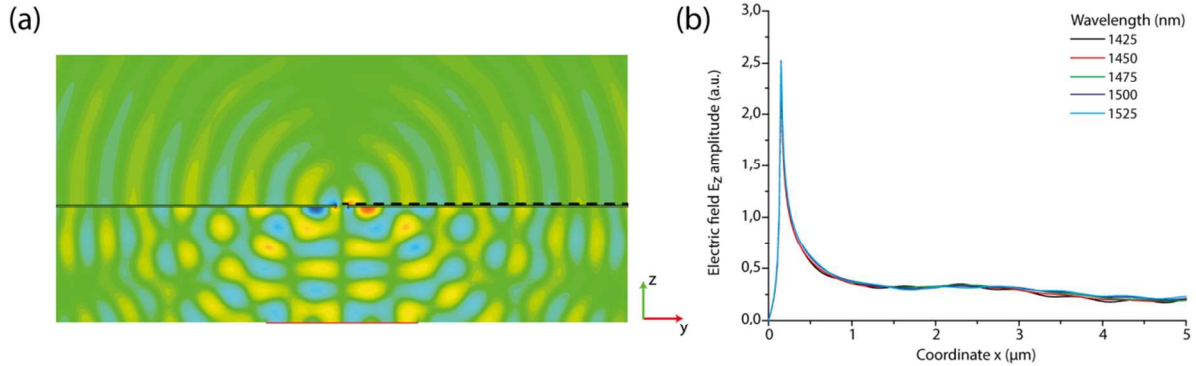


**Figure S2.** (a) Vertical electric field  $E_z$  (real part) distribution in the plane perpendicular to the slot. The y-polarized incident wave excites SPP on the air-metal interface upon diffraction through the slot. (b) Electric field  $E_z$  amplitude along the dashed line in the part (a) demonstrates that the intensity of the excited SPP does not significantly depend on the wavelength.

**Fabrication.** The waveguides and antennas were fabricated on a borofloat glass 500 $\mu\text{m}$  thick substrate (Jinsol). ZEP 520 5.5% (in anisole) resist (thickness 150 nm) was used for electron beam lithography. To prevent charge accumulation a 20 nm thick Al layer was thermally deposited (Wordentec QCL 800). The resist was exposed with 100 kV JEOL JBX-9300FS electron beam lithography system at the charge dose 200  $\mu\text{C}/\text{cm}^2$ . Then Al was removed with commercial MF-322 remover until no visible signs of metal were presented, and the resist was developed in ZED N50 developer for 120 s. Then 1 nm Cr and 49 nm Au were e-beam evaporated (Wordentec QCL 800). During the lift-off the sample was staying in hot acetone (50 C) upside down for 2 hours under constant stirring. Then slight ultrasound was applied for 2 minutes. Finally the sample was rinsed with acetone and isopropanol and carefully dried with nitrogen. After the fabrication we performed lateral size measurements with a scanning electron microscope (FEI Nova 600 NanoSEM and SEM Zeiss Supra 40 VP) and thickness measurements with an atomic force microscope (Dimension 3100 Bruker AXS). The values of the geometrical parameters of the fabricated structures and standard deviations are shown in Table S1. The SEM images of 0BA, 2BA and 2DA structures are shown in Figure S3.

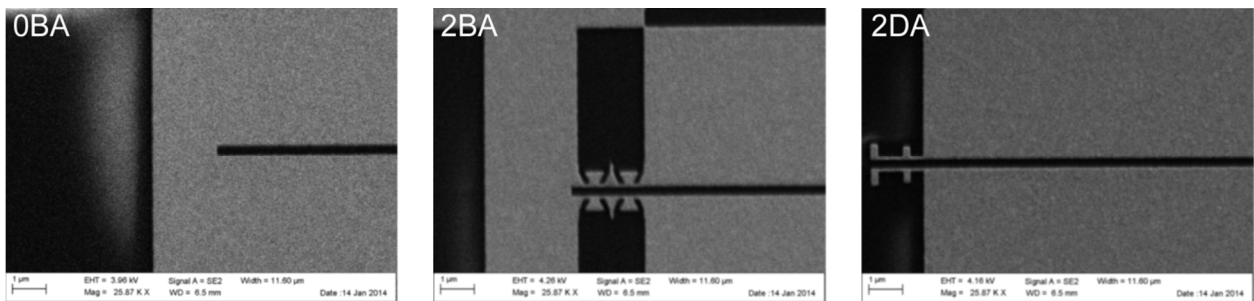


**Figure S3.** SEM microphotographs of the fabricated 0BA, 2 BA and 2DA structures.

**Field data processing.** A main idea of filtering near-field data is that the recorded field resulted from the interference of two dominating modes: the slot mode propagating along the

waveguide, and SPP, excited on the edges of the waveguide and therefore travelling across it. However, there is a small difference in treating experimental and simulated near-fields, due to a slightly different excitation and measurement procedures. In our experiment the waveguides were illuminated with a defocused Gaussian beam, which can be described as following:

$$E(x, y) = E_0 \exp\left[-\frac{x^2 + y^2}{w^2(z)}\right] \exp\left[ik_0 \frac{x^2 + y^2}{2R(z)}\right] = E_0 \exp\left[ik_2(x^2 + y^2)\right],$$

$$\left. \begin{aligned} w^2(z) &= w_0^2 \left[ 1 + \left( \frac{z}{z_R} \right)^2 \right] \\ R(z) &= z \left[ 1 + \left( \frac{z_R}{z} \right)^2 \right] \end{aligned} \right\} k_2 = \frac{k_0}{2R(z)} + \frac{i}{w^2(z)},$$

$$z_R = \frac{\pi w_0^2}{\lambda}, \quad k_0 = \frac{2\pi}{\lambda}$$

where  $E_0$  is an electric field amplitude,  $\lambda$  is a free-space wavelength of illumination,  $w_0 \approx 3 \mu\text{m}$  is a waist of the Gaussian beam, and  $z \approx 65 \mu\text{m}$  is a vertical shift of the excitation parabolic mirror, used to increase the width of the illumination spot. Since only the sample is moving during the scan, the amplitude and phase of the Gaussian beam adjusted with the AFM tip will be changed at the position of the antenna during the scan change. Therefore, the measured amplitude of the slot mode will be in fact a convolution of the Gaussian beam profile and real propagation field. Then one can fit measured data with following:

$$E_{\text{measured}}(x, y) \rightarrow E_{\text{SPP}}(y) + E_{\text{slot}}(y) \exp[ik_{\text{slot}}x] \exp\left[ik_2(x - x_0)^2\right]$$

where  $E_{\text{measured}}$ ,  $E_{\text{SPP}}$ ,  $E_{\text{slot}}$ ,  $k_{\text{slot}}$ ,  $k_2$  are complex-valued functions and variables (taking into account amplitude and phase for  $E$ -field and propagation with decay for the  $k$ -vector), and  $x_0$  is an effective coordinate of the antenna (in our fitting we assumed it to be  $1 \mu\text{m}$  from the edge of continuous gold for 2BA and 2DA; for 0BA it was assumed to be at the beginning of the waveguide). In our fitting  $k_{\text{slot}}$  was a global fitting parameter (one for the whole image), while

$E_{\text{SPP}}$  and  $E_{\text{slot}}$  were fitting parameters for each line along x-axis. The fitting was done in MATLAB by the least squares method with a use of the built-in MATLAB function *lsqcurvefit*. The results of the fitting for 2DA are shown in Figure S4, where the measured data,  $E_{\text{measured}}(x, y)$  is denoted as RAW, the first term of fitting,  $E_{\text{SPP}}(y)$ , is denoted as SPP, the second term,  $E_{\text{slot}}(y) \exp[ik_{\text{slot}}x] \exp[ik_2(x-x_0)^2]$ , is denoted as Slot mode, and the difference,  $E_{\text{measured}}(x, y) - E_{\text{SPP}}(y) - E_{\text{slot}}(y) \exp[ik_{\text{slot}}x] \exp[ik_2(x-x_0)^2]$ , as Residual field.

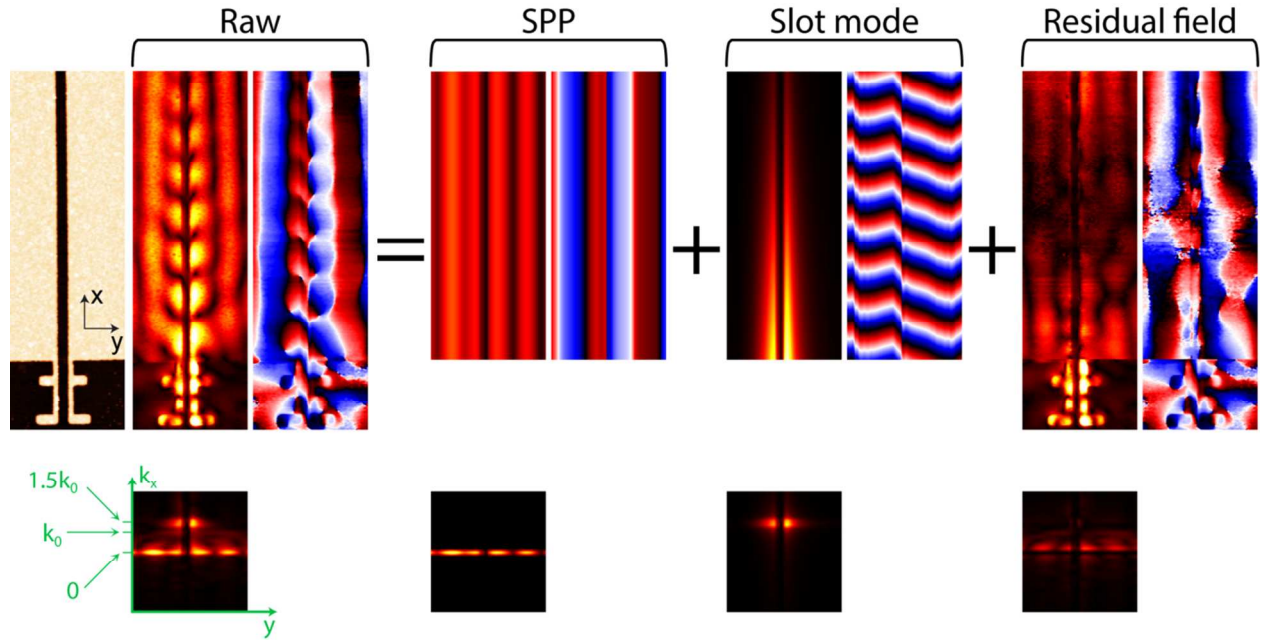


**Figure S4.** Fitting procedure shown on an example of 2DA. Top: Decomposition of the recorded Raw complex-valued data into fitted SPP, Slot mode, and Residual field. Bottom: the same procedure seen in k-space after applying 1D DFT along the waveguide ( $191 \times 31$  pixels, linearly interpolated to  $191 \times 200$  pixels for clarity).

In order to present results concisely, we added the top part of Residual field (containing the waveguide) to SPP and showed it as the SPP background in our work [Figure 4 (e)-(g)], while the original near-field of the antenna (bottom part without waveguide), glued with fitted Slot

mode, is referred to as the slot mode field in our work [Figure 4 (h)-(j)]. The complete procedure of fitting is shown in Figure S4. One can note that there is still relatively large residual field near the beginning of the waveguide, which we ascribe to the excitation and propagation of the SPP, travelling partially along  $x$ -axis, due to the diffraction of the incident beam on the antenna and due to the edge effects for SPP, propagating across the waveguide. However, such distortion does not significantly influence the fitted slot mode and the filtering procedure, which is verified by a one-dimensional discrete Fourier transform (1D DFT) of the top part of complex-valued Raw, SPP, Slot mode, and Residual field along the waveguide (see bottom part of Figure S4). Note that due to a rather limited scanned area Fourier analysis does not allow to accurately determine waveguiding propagation constant  $k_{\text{slot}}$ .

Such fitting allowed determining propagation length and effective mode index of the slot mode for each wavelength [Figure 6(b)]. The normalized intensity of the slot mode was estimated as average value of squared  $E_{\text{slot}}$ , measured at the entrance of waveguide,  $x_1$ , and normalized to the average value of squared  $E_{\text{SPP}}$ , i.e.,

$$I_{\text{slot}} = \frac{\int E_{\text{slot}}(y) \exp[ik_{\text{slot}}x_1] \exp\left[ik_2(x_1 - x_0)^2\right] dy}{\int E_{\text{SPP}}(y) dy}.$$

For 0BA, due to a weak slot mode,  $k_{\text{slot}}$  was fixed and determined by linear fitting of  $k_{\text{slot}}$  for 2DA and 2BA, so only the normalized intensity was determined during the fitting procedure.

As for the numerical simulations with plane wave excitation, the electrical field  $E_z$ , measured at 50 nm above the structure, appeared to contain substantial background of propagating light and SPP, excited on far edges of the sample due to diffraction. Such background negligibly influences the measurements of propagation constant and coupling efficiency, but creates a large obstacle for field filtering. Therefore, for near-field simulations, we used a cylindric Gaussian

beam (homogenous along x- and Gaussian along y-axis) to excite slot mode and cross-propagating SPP. The complete results of fitting the experimentally measured and numerically simulated near-field are presented in Figures S5 and S6, correspondingly.

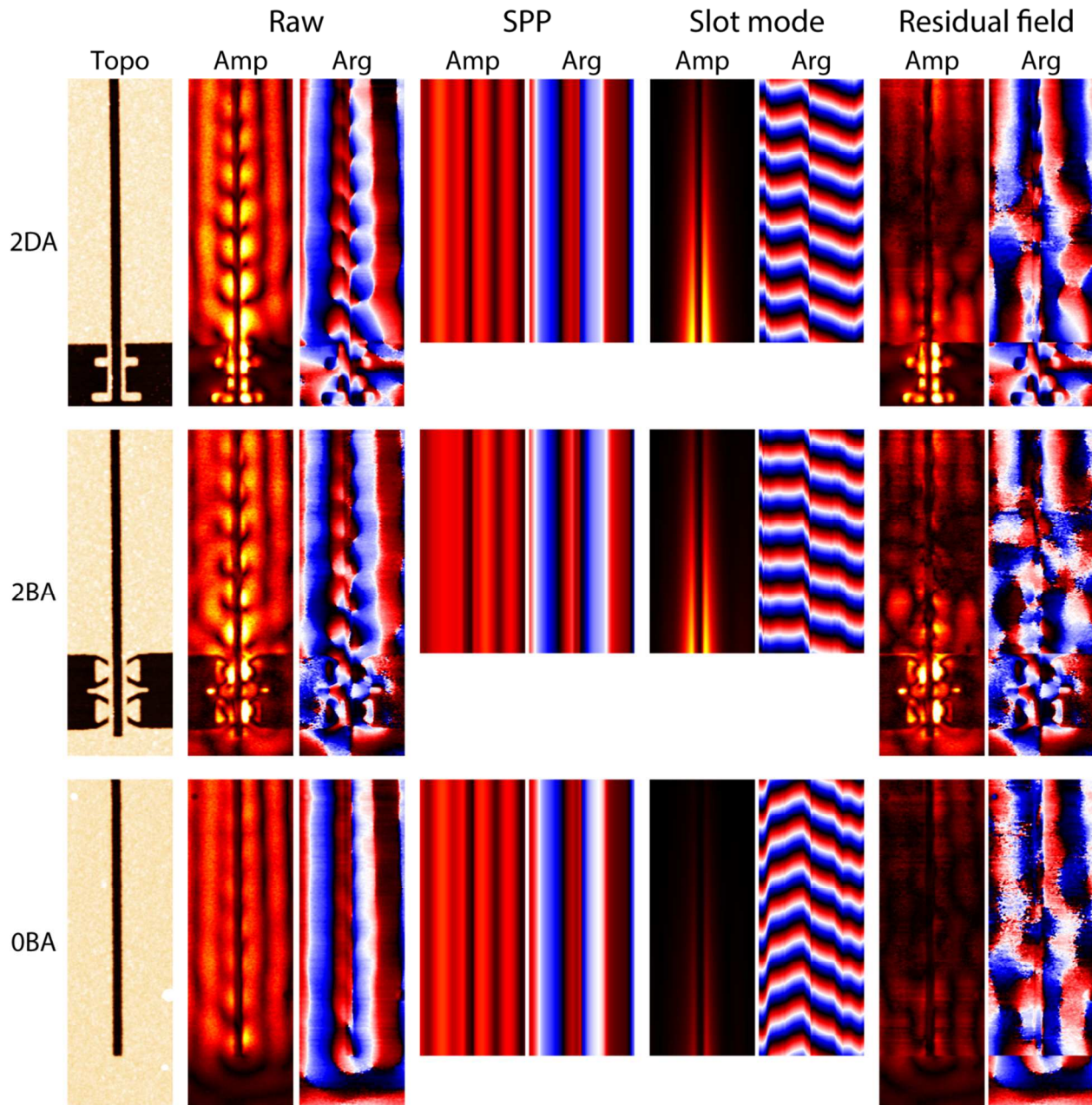


**Figure S5.** Results of fitting measured data for all measured antennas.

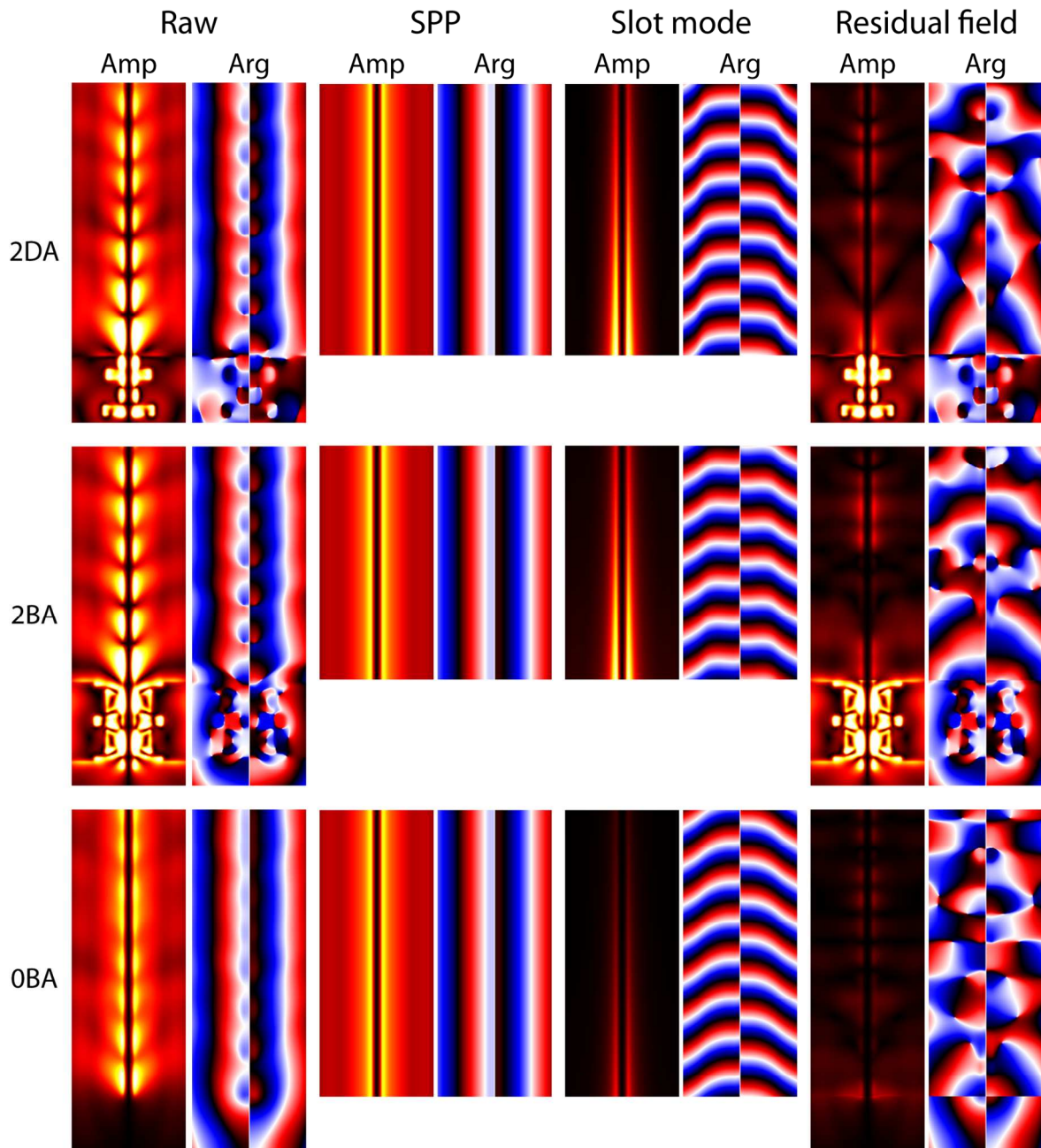


**Figure S6.** Results of fitting numerically simulated near-field.

### References

- (1) CST. Computer Simulation Technology, AS <http://cst.com>.
- (2) Rakic, A D.; Djurisic, A. B.; Elazar, J. M.; Majewski, M. L.; Djuris, A. B. *Appl. Opt.* **1998**, *37*, 5271–5283.